Volume 1 | Number 1 | Jan 2013 | Pages 1–100

ChemComm

Chemical Communications
www.rsc.org/chemcomm

ROYAL SOCIETY OF CHEMISTRY

This is an *Accepted Manuscript*, which has been through the Royal Society of Chemistry peer review process and has been accepted for publication.

Accepted Manuscripts are published online shortly after acceptance, before technical editing, formatting and proof reading. Using this free service, authors can make their results available to the community, in citable form, before we publish the edited article. We will replace this *Accepted Manuscript* with the edited and formatted *Advance Article* as soon as it is available.

You can find more information about *Accepted Manuscripts* in the **Information for Authors**.

Please note that technical editing may introduce minor changes to the text and/or graphics, which may alter content. The journal's standard **Terms & Conditions** and the **Ethical guidelines** still apply. In no event shall the Royal Society of Chemistry be held responsible for any errors or omissions in this *Accepted Manuscript* or any consequences arising from the use of any information it contains.

www.rsc.org/chemcomm

ChemComm

Dynamic Article Links ▶

COMMUNICATION

Li-Rich Anti-Perovskite Li₃OCl Films with Enhanced Ionic Conductivity

Xujie Lü,*[ab] Gang Wu,[a] John W. Howard,[ab] Aiping Chen,[a] Yusheng Zhao,*[b] Luke L. Daemen,[a] and Quanxi Jia*[a]

Anti-perovskite solid electrolyte films were prepared by pulsed laser deposition, and their room-temperature ionic conductivity can be improved by more than an order of
10 **magnitude in comparison with its bulk counterpart. The cyclability of Li₃OCl films in contact with lithium was evaluated using a Li/Li₃OCl/Li symmetric cell, showing self-stabilization during cycling test.**

Lithium ion batteries (LIBs) have found wide applications in
15 technologically important areas because of their high energy density, power capacity, charge-discharge rate, and long cycling lifetime.[1-5] However, the liquid electrolytes currently used in LIBs are composed of lithium salts dissolved in solvents and they are often toxic, corrosive, and flammable. These safety issues
20 have to be considered in practical applications.[6, 7] Replacing liquid electrolytes with solid electrolytes can avoid those shortcomings and can be integrated with a metallic lithium anode, allowing all-solid-state LIBs with potentially high energy and power densities. Nevertheless, solid electrolytes have not been
25 extensively used in lithium batteries because their ionic conductivities are still too low to meet the requirements for efficient electric-energy storage.[8-10] In addition, high interfacial resistance between the solid electrolyte and electrode is yet another challenge for solid-state LIBs.
30 Different lithium-ion-conducting materials such as Li_3PS_4 and $Li_7La_3Zr_2O_{12}$ have been explored as solid electrolytes,[11-13] but their ionic conductivities are still a few orders of magnitude lower than those of the liquid electrolytes. Achieving a high ionic conductivity of solid electrolytes is a formidable task in the
35 development of solid-state LIBs. Recently, lithium-rich anti-perovskite (LiRAP), Li_3OX (X = Cl, Br, *etc.*), has been reported as 3D-conducting solid Li-ion electrolytes potentially for high performance solid batteries.[14] This class of materials can accommodate a large number of mobile Li ions in the crystal
40 lattice and has a low energy barrier for ionic transport. By cation or anion doping, LiRAP can reach an ionic conductivity of 10^{-3} S cm^{-1} at room temperature and even higher values at elevated temperatures. For example, the ionic conductivity of Li_3OCl has been measured to be 0.85×10^{-3} S cm^{-1} at room temperature and
45 4.82×10^{-3} S cm^{-1} at 250 ℃.[14] Besides high ionic conductivity and low activation energy for Li transport, LiRAP has some other advantages including (1) low electronic conductivity with minimum self-discharge for long shelf life (band gap exceeds 5

eV for Li_3OCl[15, 16]); (2) stable operation at high temperature up to
50 275 °C; (3) large electrochemical working windows; and (4) environmental friendliness.

Thin-film LIBs, due to their high volumetric energy density and agility to be fabricated into different shapes and sizes on different substrates, may find numerous applications in portable
55 devices such as cellular phones, computers, and smart cards where on-chip power sources with high energy density is mandatory.[17-19] To fabricate thin-film LIBs, it is necessary to deposit desired anode, cathode, and electrolyte materials into film format, most importantly to form multilayered films with good
60 structural integrity and controllable interfaces. The formation of solid electrolyte films is one of the key steps to ensure high ionic conductivity of the electrolyte layer and low interfacial resistances, subsequently achieving high performance of solid thin-film Li batteries. As of now, there are very limited reports on
65 the preparation and characterization of solid electrolytes in the form of thin films. Herein, we report the fabrication of Li-rich anti-perovskite Li_3OCl solid electrolyte films *via* pulsed laser deposition (PLD) for the first time. The ionic conductivities of Li_3OCl films were evaluated by electrochemical impedance
70 spectroscopy (EIS) at various temperatures. The long-term stability and compatibility of the Li_3OCl films with Li and Ag electrodes were investigated by testing symmetric cells of both Li/Li₃OCl/Li and Ag/Li₃OCl/Ag.

The Li_3OCl films were deposited on $LaAlO_3$ (LAO), Ag or Li
75 coated stainless steel substrates by PLD (KrF laser, 248 nm, 20 Hz) under vacuum using a home-made Li_3OCl target (see experimental details in ESI†). Tri-layer films of Ag/Li₃OCl/Ag and Li/Li₃OCl/Li were constructed to study the electrochemical properties. Electrochemical tests were carried out using a
80 specially designed air-tight cell. AC impedance spectroscopy measurements were conducted in the frequency range of 1 Hz to 1 MHz with an amplitude of 10 mV. The symmetric cells were cycled on a battery test station by applying a constant current of 100 μA with periodically changed polarity at room temperature.
85 The formation of anti-perovskite Li_3OCl is verified by the X-ray diffraction (XRD). As shown in Fig. 1, the peak at 2θ = 23.5º belongs to the LAO (001) substrate. The peak at 2θ = 32.7º can be indexed as (011) of the cubic Li_3OCl phase with the space group of *Pm3m* and lattice constant of 3.91Å (the crystal
90 structure of cubic Li_3OCl is shown in the inset of Fig. 1). The XRD pattern of the film in comparison with that of the target

ChemComm Accepted Manuscript

material is shown in Fig. S1 in ESI†. These XRD results indicate the preferential orientation of the PLD-fabricated Li_3OCl film.
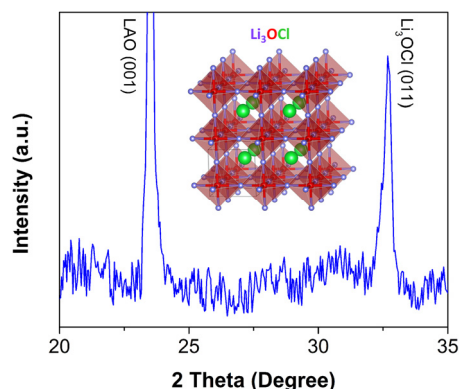
Fig. 1 XRD pattern of Li_3OCl film on LAO substrate. The inset shows the crystal structure of anti-perovskite cubic Li_3OCl.

Considering the moisture-sensitivity of the anti-perovskite Li_3OCl, we have to protect the films during the post-processes and conduct the electrochemical measurements in a dry environment. A tri-layer film of $Ag/Li_3OCl/Ag$, with Ag coating as both a protective layer and a conductive electrode, was constructed by PLD without breaking the vacuum during deposition. In order to further protect these films, as shown in Fig. 2a, a design based on a CR2032 coin cell is employed to conduct the electrochemical measurements of Li_3OCl films. Using this configuration, both electrochemical impedance and cycling measurements can be performed outside of the glove box, because the air-tight coin cell cases prevent the films from exposure to atmospheric moisture.
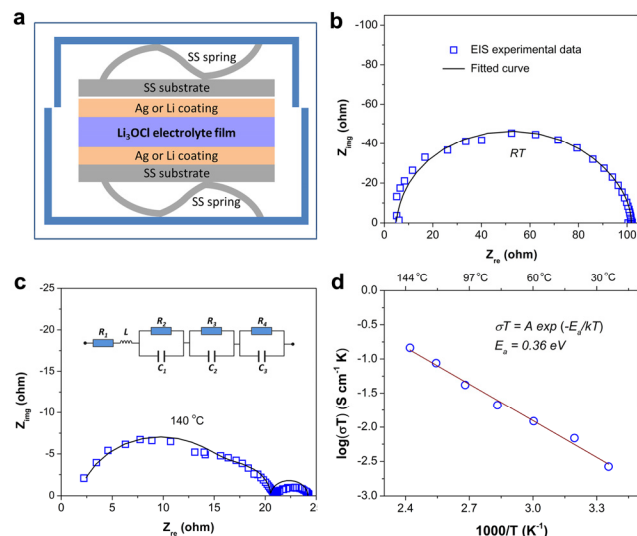
Fig. 2 (a) A design based on the CR2032 coin cell for electrochemical measurements of PLD-fabricated Li_3OCl films; (b), (c) EIS Nyquist plots measured at room temperature and 140 °C, and the corresponding fitted curves; (d) Arrhenius plot for Li_3OCl film. The activation energy E_a is derived by the slope of the linear fitting of $\log(\sigma T)$ versus 1000/T.

Two typical impedance spectra measured at room temperature and 140 °C are presented as Nyquist plots in Fig. 2b & c. Inset of Fig. 2c shows the equivalent circuit of the cell. The ionic conductivity of Li_3OCl film was measured to be 8.9×10^{-6} S cm^{-1} at room temperature, which is much higher than that of the

ceramic bulk Li_3OCl used as the source material for target (5.8×10^{-7} S cm^{-1}). The intimate contact among the grains of the Li_3OCl film may contribute to such a higher ionic conductivity of the films. As the temperature reached to 140 °C, the conductivity value reached to 3.5×10^{-4} S cm^{-1}. As shown in Fig. 2d, the ionic conductivities of Li_3OCl film at different temperatures follow typical Arrhenius behavior, which reflects an increase of the ionic conductivity with temperature in an exponential manner described by $\sigma T = A \times exp(-E_a/kT)$, where σ is the ionic conductivity, E_a is the activation energy for ion transport in the crystal lattice, k is the Boltzmann constant ($k = 8.617 \times 10^{-5}$ eV K^{-1}), and A is the pre-exponential factor. The E_a derived from the slope of the fitted curve is 0.36 eV, lower than a value of 0.59 eV for the bulk Li_3OCl material used for target (see Fig. S2 in ESI†).

It is worth noting that the conductivity of bulk Li_3OCl used in this study is lower than the previously reported value.[14] In that work, the samples were heat-treated at 360 °C for a long period of time (~100 hours). It is possible that the volatile elements such as lithium and chlorine can escape from the crystal lattice during this process, resulting in the formation of a "depleted" anti-perovskite denoted as $Li_{3-\delta}OCl_{1-\delta}$. Deficiencies of Li^+ and/or Cl^- can potentially lead to enhanced conductivity in comparison with the stoichiometric Li_3OCl. Furthermore, the melted electrolytes may react with the aluminum foil during cell fabrication and inadvertently dope the anti-perovskite with Al^{3+} cation, inducing a high concentration of vacancies at the octahedral vertices due to the charge-balance rule.[14] We believe that the vacancies of Li^+ and/or Cl^- and the dopants of Al^{3+} are the main reasons for the significantly higher ionic conductivity reported in the reference.[14]

Presumably, the Li^+ and Cl^- vacancies may also be the reason for the higher conductivity of the Li_3OCl film than that of the bulk material, because our Li_3OCl films were deposited under vacuum. Using *ab initio* simulation, Zhang *et al*. have reported that the LiRAPs with a perfect crystal structure are not good Li-ion conductors, and vacancies promote Li-ion migration by reducing the enthalpy barriers along the preferred pathways.[16] An analysis of the simulation results indicates that the nearest-neighbor Li-ion hopping occurs along the edge of the Li_6O octahedron *via* Li vacancies, *i.e.*, along the (011) planes (as shown in Fig. S3 in ESI†). This mechanism can explain the experimental results where Li vacancies were introduced during synthesis, resulting in the formation of non-stoichiometric Li_3OCl with enhanced ionic conductivity. Systematical studies on the effects of doping, depleting, and mixing on the properties of Li_3OCl are underway. Our preliminary results show that both the doped and non-stoichiometric materials possess improved ionic conductivity, which is in agreement with the simulation results.[16] The change in the slope of the linear fitted Arrhenius curve denotes a change in activation energy for Li transport (0.36 eV for Li_3OCl film and 0.59 eV for bulk material). The reduction of the activation energy is most likely an indication of structural change (octahedral tilting caused by Li^+ & Cl^- depleting, preferential orientation of the films, *etc*.), grain boundary change, and increase of migration vacancies.

Besides the ionic conductivity, we have measured the cyclability and compatibility of Li_3OCl film in contact with metallic Li using a symmetric cell of $Li/Li_3OCl/Li$ by applying a

constant direct-current (DC) with periodically changed polarity. Fig. 3a shows the voltage profile of the cell cycled continuously for 65 hours (1 hour per cycle) at room temperature.

As can be seen from Fig. 3a, the cell shows a voltage of about 6 mV at a constant current of 100 μA in the first cycle. The 10 voltage keeps increasing (due to the increase of resistance) during cycling tests, especially in the first 20 cycles. However, the increasing rate decreases with time, which implies the self-stabilizing feature of this system. On the other hand, no voltage increase can be observed for the symmetric Ag/Li$_3$OCl/Ag cell 15 during the cycling test from the beginning up to 65 cycles (see Fig. 3b), indicating that the Li$_3$OCl film itself is stable. Thus we speculate that there are some interactions between Li and Li$_3$OCl at their interfaces, which may be caused by the oxidation of Li metal by the oxygen from Li$_3$OCl electrolyte or other oxygen 20 sources. Nevertheless, the cell could reach a stable state after certain numbers of cycling tests. It should be noted that superior stability and compatibility of the bulk anti-perovskite Li$_3$OCl electrolytes with Li metal have been verified using the same symmetric cells in our experiments (not shown here). The 25 different behaviors between the films and bulk materials may be due to the thickness effect. The contribution of interfacial resistances in the films with a thickness of about 2 μm is much more pronounced than that of the bulk samples with a thickness of about 2 mm. So the interactions between Li and bulk Li$_3$OCl at 30 their interfaces may not have an obvious effect on the overall resistance.

Conclusions

In conclusion, anti-perovskite Li$_3$OCl films with an enhanced ionic conductivity were deposited by pulsed laser deposition at 35 temperatures lower than 300 ^{o}C. The ionic conductivities of the Li$_3$OCl films were determined to be 8.9×10^{-6} S cm^{-1} at room temperature and 3.5×10^{-4} S cm^{-1} at 140 ^{o}C. The temperature-dependent conductivity of the films can be well fitted by the Arrhenius equation with an activation energy of 0.36 eV. The 40 ionic conductivity of the Li$_3$OCl film is more than one order of magnitude higher than that of the bulk Li$_3$OCl materials, which may be attributed to the Li$^+$ and/or Cl$^-$ vacancies and also the preferential orientation of the film. Cyclability and compatibility of Li$_3$OCl film with Li metal were measured using a symmetric 45 cell of Li/Li$_3$OCl/Li, showing the increase of resistance initially and then self-stabilized at a certain value. The anti-perovskite Li$_3$OCl electrolyte films with enhanced ionic conductivity hold great promise for battery applications where high-level safety and high energy density are required, such as electric vehicles.

Notes and references

^{a} *Los Alamos National Laboratory, Los Alamos, New Mexico 87545,*
60 *USA. Fax: 1-(505) 665-9030; Tel: 1-(505) 665-9399; E-mail:*
xujie@lanl.gov, qxjia@lanl.gov
^{b} *University of Nevada, Las Vegas, Nevada 89154, USA. E-mail:*
yusheng.zhao@unlv.edu
† Electronic Supplementary Information (ESI) available: Experimental 65 details, and Arrhenius plot for bulk Li$_3$OCl (target material). See DOI: 10.1039/b000000x/

1. J. B. Goodenough and K.-S. Park, *J. Am. Chem. Soc.*, 2013, **135**, 1167-1176.
70 2. H. Li, Z. Wang, L. Chen and X. Huang, *Adv. Mater.*, 2009, **21**, 4593-4607.
3. B. Scrosati, *Electrochim. Acta*, 2000, **45**, 2461-2466.
4. Y. Wang, J. Wu, Y. Tang, X. Lü, C. Yang, M. Qin, F. Huang, X. Li and X. Zhang, *ACS Appl. Mater. Interfaces*, 2012, **4**, 4246-4250.
75 5. H. Li and H. Zhou, *Chem. Commun.*, 2012, **48**, 1201-1217.
6. V. Etacheri, R. Marom, R. Elazari, G. Salitra and D. Aurbach, *Energy Environ. Sci.*, 2011, **4**, 3243-3262.
7. J. B. Goodenough and Y. Kim, *Chem. Mater.*, 2009, **22**, 587-603.
8. P. Verma, P. Maire and P. Novák, *Electrochim. Acta*, 2010, **55**, 6332-80 6341.
9. Q. Zhang, N. Schmidt, J. Lan, W. Kim and G. Cao, *Chem. Commun.*, 2014, **50**, 5593-5596.
10. G. Sahu, Z. Lin, J. Li, Z. Liu, N. Dudney and C. Liang, *Energy Environ. Sci.*, 2014, **7**, 1053-1058.
85 11. Z. Liu, W. Fu, E. A. Payzant, X. Yu, Z. Wu, N. J. Dudney, J. Kiggans, K. Hong, A. J. Rondinone and C. Liang, *J. Am. Chem. Soc.*, 2013, **135**, 975-978.
12. M. Kotobuki, H. Munakata, K. Kanamura, Y. Sato and T. Yoshida, *J. Electrochem. Soc.*, 2010, **157**, A1076-A1079.
90 13. J. Han, J. Zhu, Y. Li, X. Yu, S. Wang, G. Wu, H. Xie, S. C. Vogel, F. Izumi, K. Momma, Y. Kawamura, Y. Huang, J. B. Goodenough and Y. Zhao, *Chem. Commun.*, 2012, **48**, 9840-9842.
14. Y. Zhao and L. L. Daemen, *J. Am. Chem. Soc.*, 2012, **134**, 15042-15047.
95 15. A. Emly, E. Kioupakis and A. Van der Ven, *Chem. Mater.*, 2013, **25**, 4663-4670.
16. Y. Zhang, Y. Zhao and C. Chen, *Phys. Rev. B: Condens. Matter*, 2013, **87**, 134303.
17. M. Koo, K.-I. Park, S. H. Lee, M. Suh, D. Y. Jeon, J. W. Choi, K. 100 Kang and K. J. Lee, *Nano Lett.*, 2012, **12**, 4810-4816.
18. J. F. Ihlefeld, P. G. Clem, B. L. Doyle, P. G. Kotula, K. R. Fenton and C. A. Apblett, *Adv. Mater.*, 2011, **23**, 5663-5667.
19. L. Hu, H. Wu, F. La Mantia, Y. Yang and Y. Cui, *ACS Nano*, 2010, **4**, 5843-5848.